

## BAYESIAN NEURAL NETWORK PRIORS FOR EDGE-PRESERVING INVERSION

CHEN LI, MATTHEW DUNLOP, AND GEORG STADLER

Courant Institute of Mathematical Sciences, New York University  
251 Mercer Street, New York, NY 10012, USA

**ABSTRACT.** We consider Bayesian inverse problems wherein the unknown state is assumed to be a function with discontinuous structure a priori. A class of prior distributions based on the output of neural networks with heavy-tailed weights is introduced, motivated by existing results concerning the infinite-width limit of such networks. We show theoretically that samples from such priors have desirable discontinuous-like properties even when the network width is finite, making them appropriate for edge-preserving inversion. Numerically we consider deconvolution problems defined on one- and two-dimensional spatial domains to illustrate the effectiveness of these priors; MAP estimation, dimension-robust MCMC sampling and ensemble-based approximations are utilized to probe the posterior distribution. The accuracy of point estimates is shown to exceed those obtained from non-heavy tailed priors, and uncertainty estimates are shown to provide more useful qualitative information.

**1. Introduction.** Inverse problems aim at inferring information about unknown parameters  $u \in \mathcal{U}$  from observations  $y \in \mathcal{Y}$  and a model that relates parameters and observations. Denoting the model by  $\mathcal{F} : \mathcal{U} \rightarrow \mathcal{Y}$  and assuming additive observation errors  $\varepsilon$ , the relation between parameters, model and observations is

$$y = \mathcal{F}(u) + \varepsilon. \quad (1)$$

In the Bayesian approach to inverse problems, one considers  $u, y$  and  $\varepsilon$  as random variables. In particular, one requires a distribution  $p(u)$  that reflects prior knowledge about the parameters  $u$ . The solution to this Bayesian inverse problem is then the posterior distribution  $p(u|y)$  of the parameters, defined via Bayes' rule as

$$p(u|y) \propto p(y|u)p(u), \quad (2)$$

where ‘ $\propto$ ’ means equality up to a normalization constant, and  $p(y|u)$  is the likelihood derived from the forward model (1) and the distribution of the errors  $\varepsilon$ . The Bayesian approach to inverse problems has a long history [16, 21]. While many important questions around the characterization of the posterior distribution remain, the main focus of this paper is on the choice of prior distributions for  $u \in \mathcal{U}$ . In particular, we are interested in problems where  $\mathcal{U}$  is a space of functions defined over a domain  $\mathcal{D} \subset \mathbb{R}^d$ , with  $d \in \{1, 2, 3\}$ , and we have the prior knowledge that the true

---

2020 *Mathematics Subject Classification.* Primary: 62F15, 68T07, 60E07; Secondary: 65C05 .  
*Key words and phrases.* Bayesian priors, Bayesian neural networks, inverse problems,  $\alpha$ -stable distribution, deblurring.

Partially supported by the US National Science Foundation under grants #1723211 and #1913129.

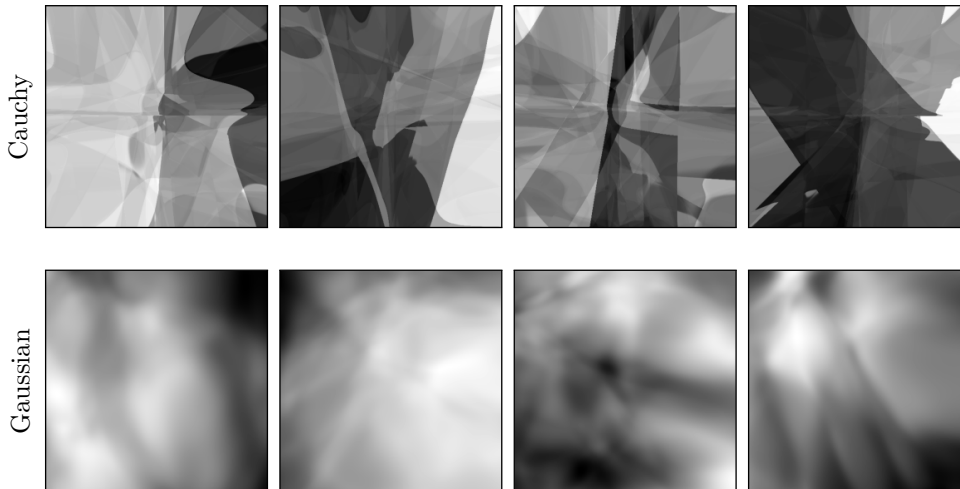


FIGURE 1. Comparison between outputs on  $[-1, 1]^2$  of Bayesian neural network priors with three hidden layers. Shown are realizations of networks with  $\tanh(\cdot)$  as activation function and Cauchy weights (top) and Gaussian weights (bottom).

parameter might be a discontinuous function over  $\mathcal{D}$ . Samples from the prior distribution  $p(u)$  should thus include discontinuous (or approximately discontinuous) functions. This is known to be a challenging problem, and the aim of this paper is to propose a novel method based on Bayesian neural network parameterizations to define  $p(u)$ .

*Approach.* We study neural network priors with weights drawn from  $\alpha$ -stable distributions as proposed in [27]. In Figure 1, we compare samples generated with such neural network priors with Cauchy and Gaussian weights, which are  $\alpha$ -stable random variables with  $\alpha = 1, 2$ . As can be seen, neural networks with Cauchy weights generate samples that have large jumps, compared to those with Gaussian weights. This behavior is due to the heavy tails of Cauchy distributions, resulting in strongly re-scaled neural network activation functions that visually appear as discontinuities in the network outputs. The prior we propose builds on this observation. To study its properties, we first summarize known theoretical results on the convergence of neural networks with  $\alpha$ -stable weights in the limit of infinite width. Then, for finite-width networks, we present results on the distribution of pointwise derivatives of the output and use them to explain the behavior shown in Figure 1. We also discuss practical methods to condition these neural network priors with observations using optimization as well as sampling methods.

*Contributions.* The main contribution of this work are as follows. (1) For finite-width networks, we prove that the distribution of the derivative of the output function at an arbitrary but fixed point is heavy-tailed provided the weights in the network are heavy-tailed. This explains the large jumps in the output function generated by certain neural networks. (2) We discuss practical methods to condition these neural network priors using observations, and present a comprehensive numerical study using image deconvolution problems in one and two space dimensions.

*Paper outline.* The outline of this work is as follows. In Sec. 2, we review existing priors for Bayesian inverse problems and introduce neural network priors with general  $\alpha$ -stable distributed weights. We provide a systematic discussion of the properties of neural network priors both in the cases of infinite width and finite width. In Sec. 3, we review the Bayesian approach for inverse problems and discuss optimization and sampling methods to explore the posterior distribution. In Sec. 4, we study the numerical performance of different neural network priors using two deblurring examples with discontinuous parameter functions. Finally, we draw conclusions and point out potential research directions in Sec. 5.

**2. Prior modeling with neural networks.** Here, we review priors for infinite-dimensional Bayesian inverse problems and study properties of neural network priors. We provide an overview of existing priors for Bayesian inverse problems in Sec. 2.1. In Sec. 2.2, we propose functions parameterized using neural networks with random weights as priors. Numerical tests motivate using neural networks with weights drawn from  $\alpha$ -stable distributions as priors for discontinuous parameter functions. We introduce  $\alpha$ -stable distributions in Sec. 2.3. In Sec. 2.4, we provide a review of the limiting properties of Bayesian neural networks with Gaussian and  $\alpha$ -stable ( $0 < \alpha < 2$ ) weights as the width of network layers goes to infinity. We present our main results on neural network priors with finite width in Sec. 2.5.

**2.1. Related literature.** We consider priors for unknown parameter functions  $u$  defined over a domain  $\mathcal{D}$ . One approach to infinite-dimensional Bayesian problems is to first discretize all functions and use a finite-dimensional perspective [11, 22]. Methods building on this approach may suffer from a dependence on the discretization, i.e., their performance may degrade as the discretization is refined. Alternatively, one can analyze and develop methods for Bayesian inverse problems in function space and then discretize them [33]. This approach typically avoids mesh dependence but is theoretically more challenging. We follow the latter approach, i.e., construct priors in function space.

Priors encode a priori available information about the unknown function  $u$ . A common choice are Gaussian priors, for which a vast number of theoretical and computational results are available [5, 30, 33]. A sample  $u$  from a Gaussian prior can be constructed using, e.g., the Karhunen-Loève expansion [30]. Let  $\{\varphi_j, \rho_j^2\}_{j=1}^\infty$  be a set of orthonormal eigenfunctions and eigenvalues of a positive definite, trace-class covariance operator  $\mathcal{C}_0 : \mathcal{U} \rightarrow \mathcal{U}$ , and let  $\{\xi_j\}_{j=1}^\infty$  be an i.i.d. sequence  $\xi_j \sim \mathcal{N}(0, 1)$ . Then

$$u := m_0 + \sum_{j=1}^{\infty} \rho_j \xi_j \varphi_j \quad (3)$$

is distributed according to  $\mathcal{N}(m_0, \mathcal{C}_0)$ , where  $m_0 \in \mathcal{U}$  is the mean. Examples of covariance operators are Matérn covariance operators and fractional inverse powers of elliptic differential operators. One can show that samples from these Gaussian priors are almost surely continuous [33]. However, this might not always be desirable. For example, in many practical problems, the unknown function  $u$  might have discontinuities. Thus, a prior that allows for discontinuous samples might be preferable to a Gaussian prior.

Several priors have been proposed to overcome the limitations of Gaussian priors. For example, total variation priors based on the total variation regularization [9, 18, 25] can be defined for a fixed discretization. However, these priors converge to

Gaussian fields as the mesh is refined, which is referred to as lack of discretization invariance in [25]. That is, total variation priors depend on the discretization, which is undesirable from an infinite-dimensional perspective. Non-Gaussian priors can also be based on generalizations of the expansion (3) with non-Gaussian coefficients. For instance, when  $\{\varphi_j\}_{j=1}^\infty$  is a wavelet basis of  $\mathcal{U}$ , Besov priors are obtained if  $\{\xi_j\}_{j=1}^\infty$  are i.i.d. random variables with probability density function  $p_\xi(z) \propto \exp(-\frac{1}{2}|z|^q)$  [13]. This results in a non-Gaussian discretization-invariant prior that is able to produce discontinuous samples. However, choosing a proper wavelet basis for Besov priors is challenging and the location of discontinuities depends on this basis [13, 24].

Due to properties related to their heavy tails,  $\alpha$ -stable processes have recently been proposed as priors [7, 34]. These can be realized by choosing for  $\{\xi_j\}_{j=1}^\infty$  in (3) i.i.d.  $\alpha$ -stable distributions. The processes are well-defined in function space [34] and due to their heavy tails, they can take on extreme values and thus incorporate large jumps. Variations of  $\alpha$ -stable processes were proposed, e.g., the Cauchy difference prior [26] and the Cauchy Markov random field [8]. Such priors are difficult to sample in high dimensional problems [26].

Priors based on neural networks have been considered [2, 27]. One ongoing research direction in constructing neural network priors are generative methods, which can tailor priors to a specific application and are then used in inference problems [1, 2]. An alternative approach is constructing Bayesian neural networks, i.e., to use neural networks to parameterize functions [27] and assume that the weights in the neural network are random variables. Here, we follow this latter approach and thus introduce Bayesian neural networks next.

**2.2. Neural network priors.** Motivated by their relation to Gaussian processes under certain conditions [14, 27], neural networks can be used to construct priors in function space. These novel priors are defined as parameterizations given by a neural network with random weights drawn from specific distributions. The network is defined on a spatial domain  $\mathcal{D} \subseteq \mathbb{R}^{D_0}$ , where  $D_0 = d$  is the dimension of the input space. Let  $\Psi(\mathbf{w}) : \mathcal{D} \rightarrow \mathbb{R}$  denote the neural network, where  $\mathbf{w}$  summarizes all weights in the neural network. The network (we only consider general fully connected networks) consists of  $L$  hidden layers and its structure is

$$\mathbf{h}^{(0)}(\mathbf{x}) = \mathbf{x}, \quad (4a)$$

$$\mathbf{h}^{(l+1)}(\mathbf{x}) = \phi\left(\mathbf{b}^{(l)} + \mathbf{V}^{(l)}\mathbf{h}^{(l)}(\mathbf{x})\right), \quad l = 0, \dots, L-1, \quad (4b)$$

$$u(\mathbf{x}) = \mathbf{V}^{(L)}\mathbf{h}^{(L)}(\mathbf{x}), \quad (4c)$$

where  $\mathbf{h}^{(l)}(\mathbf{x})$  is the  $l$ -th hidden layer vector with width  $D_l$ . The matrices  $\mathbf{V}^{(l)} \in \mathbb{R}^{D_{l+1} \times D_l}$ , for  $0 \leq l < L$ , and  $\mathbf{V}^{(L)} \in \mathbb{R}^{1 \times D_L}$  are the weights of the  $l$ -th hidden layer and the output layer, respectively, and  $\mathbf{b}^{(l)} \in \mathbb{R}^{D_{l+1} \times 1}$  is the bias of the  $l$ -th hidden layer. We denote the output of the neural network as  $u(\mathbf{x})$  for input  $\mathbf{x}$ . Note that, in general,  $u$  can be vector-valued, but for simplicity we consider only scalar-valued  $u$  in this paper. The function  $\phi : \mathbb{R} \rightarrow \mathbb{R}$  denotes a nonlinear activation function in the neural network, which acts on vectors component-wise. We will mainly use the hyperbolic tangent function  $\tanh(\cdot)$  as activation in this paper. Since this is a smooth function, the input-to-output mapping of the neural network is smooth too. In particular, while samples generated by these networks

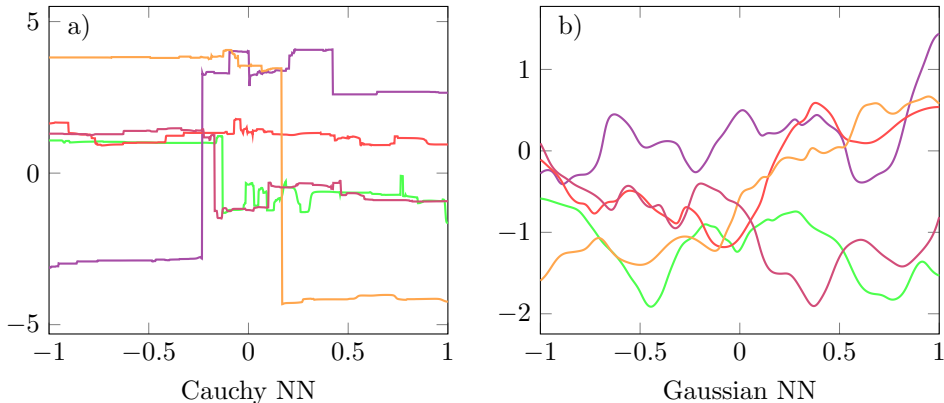


FIGURE 2. Realizations of the neural network with two different weight distributions on the interval  $[-1, 1]$ . Shown are realizations with Cauchy weights (a) and Gaussian weights (b).

appear to be discontinuous, they are continuous but have very sharp jumps that visually appear to be discontinuities.

We consider priors parameterized using (4) with weights  $\mathbf{w}$  drawn from certain distributions. Such neural network priors are flexible; one can change the distributions on the weights or the number and widths of the hidden layers to obtain different priors. One choice of weight distribution is Gaussian [27, 35], but non-Gaussian weights have also been studied [15, 27]. In this paper, we consider neural network priors with weights drawn from  $\alpha$ -stable distributions ( $0 < \alpha \leq 2$ ), in particular, Cauchy and Gaussian distributions (i.e.,  $\alpha = 1$  or  $\alpha = 2$ ).

To illustrate the difference between neural network priors with Cauchy and Gaussian weights, we show realizations from both neural networks in one dimension in Figure 2. Here, we use the neural network structure in (4) with three hidden layers of widths  $[80, 80, 100]$ . The distributions assigned to the weights are the standard Cauchy and Gaussian distributions. We observe that the realizations of the neural network prior with Cauchy weights have large jumps while realizations with Gaussian weights tend to be smooth. This is the same behavior as observed in two dimensions in Figure 1.

Note that realizations of neural network priors tend to exhibit larger variations closer to the origin, i.e., the resulting processes are non-stationary. To illustrate why this is the case, we consider a simplified neural network with a one-dimensional input, one hidden layer, and  $V^{(0)} \in \mathbb{R}^{D_1}$  is a vector of all ones:

$$u(x) = \sum_{i=1}^{D_1} V_i^{(1)} H(x - b_i^{(0)}),$$

where the activation function  $H$  is taken to be the Heaviside function for illustration purposes. For fixed biases  $b_i^{(0)}$ , the network output is a random walk with jumps occurring at each  $b_i^{(0)}$  with magnitude  $V_i^{(1)}$ . Thus, if the biases  $b_i^{(0)}$  are concentrated around zero (as in a Cauchy or Gaussian distribution), more jumps occur near the origin. If one wishes to reduce this non-stationarity,  $b_i^{(0)}$  could be taken to be uniformly distributed in some zero-centered interval. However, this will not guarantee stationarity for more general networks.

**2.3.  $\alpha$ -stable distributions.** In the previous section, we reviewed neural networks and how to consider their outputs as priors for Bayesian inverse problems. Before moving to the theoretical discussion of neural network priors with  $\alpha$ -stable weights ( $0 < \alpha \leq 2$ ), we review scalar  $\alpha$ -stable distributions.

First introduced by Lévy,  $\alpha$ -stable distributions are a class of heavy-tailed distributions, which have a large probability of attaining extreme values. Given scalars  $\alpha \in (0, 2]$  (the stability parameter) and  $\gamma > 0$  (the scaling parameter), the  $\alpha$ -stable distribution  $\text{St}(\alpha, \gamma)$  may be defined by its characteristic function

$$\Phi(t) = \mathbb{E}[\exp(it\text{St}(\alpha, \gamma))] = e^{-\gamma^\alpha |t|^\alpha}.$$

Additional parameters representing skew and location may also be introduced, though we consider these fixed at zero in this article. The absolute moment of an  $\alpha$ -stable random variable  $\text{St}(\alpha, \gamma)$ , i.e.,  $\mathbb{E}[|\text{St}(\alpha, \gamma)|^\beta]$ , is finite when  $\beta \in [0, \alpha)$  and infinite when  $\beta \in [\alpha, \infty)$ . A key property of  $\alpha$ -stable distributions is that they are closed under independent linear combinations [4] leading to generalizations of central limit theorems beyond the Gaussian regime [17].

Note that  $\text{St}(2, \gamma)$  coincides with  $\mathcal{N}(0, 2\gamma^2)$ , i.e., a mean-zero Gaussian random variable. Another special case of an  $\alpha$ -stable distribution is the Cauchy distribution for  $\alpha = 1$ . It has the probability density function

$$f(x; \gamma) = \frac{1}{\pi\gamma} \left( \frac{\gamma^2}{x^2 + \gamma^2} \right),$$

where the scaling parameter  $\gamma$  specifies the half-width at half-maximum (HWHM). In general, for  $\alpha \neq 1, 2$ , the density of  $\text{St}(\alpha, \gamma)$  may not be expressed analytically.

As discussed above, we construct different neural network priors by using different  $\alpha$ -stable distributions ( $0 < \alpha \leq 2$ ) on the weights. Gaussian and Cauchy neural network priors are obtained for  $\alpha = 1, 2$ , respectively. It is possible to define neural network priors with weights drawn from general  $\alpha$ -stable distributions, but in practice this is complicated by the lack of analytic forms. In the following, we study theoretical results for general  $\alpha$ -stable distributions but only show numerical experiments from neural network priors with Gaussian and Cauchy weights.

**2.4. Output properties of infinite-width neural network priors.** We have seen that realizations of neural networks with Cauchy weights have jumps, while realizations of networks with Gaussian weights tend to be smooth; see Figures 1 and 2. In this section, we review the convergence of neural networks with different weight distributions in the limit of infinite width [14, 27]. The results are stated for Gaussian ( $\alpha = 2$ ) and  $\alpha$ -stable distributions ( $0 < \alpha < 2$ ).

**2.4.1. Gaussian weights.** Here we summarize theoretical results for Gaussian neural networks as the widths of the hidden layers approach infinity. We start with the case of one hidden layer, i.e., (4) has the form

$$h_i^{(1)}(\mathbf{x}) = \phi \left( b_i^{(0)} + \sum_{j=1}^{D_0} V_{ij}^{(0)} x_j \right), \quad (5a)$$

$$u_{D_1}(\mathbf{x}) = \frac{1}{\sqrt{D_1}} \sum_{i=1}^{D_1} V_i^{(1)} h_i^{(1)}(\mathbf{x}), \quad (5b)$$

where  $V_{ij}, b_i, h_i$  are the components of  $\mathbf{V}, \mathbf{b}, \mathbf{h}$ , respectively. We denote the  $j$ -th component of  $\mathbf{x}$  as  $x_j$ . The normalization factor  $\frac{1}{\sqrt{D_1}}$  could also be absorbed into

the variance of the Gaussian distribution. Then, for Gaussian weights, the output converges to a Gaussian distribution when the width of the hidden layer goes to infinity, as summarized in the following theorem from [27].

**Theorem 2.1.** *Consider the neural network (5) with all weights following Gaussian distributions, i.e.,  $V_{ij}^{(0)}, V_i^{(1)} \stackrel{iid}{\sim} \mathcal{N}(0, \sigma_V^2)$ ,  $b_i^{(0)} \stackrel{iid}{\sim} \mathcal{N}(0, \sigma_b^2)$ . Assume that the activation function  $\phi(\cdot)$  is bounded and fix the input  $\mathbf{x}$ . Then, as the width  $D_1 \rightarrow \infty$ , the output  $u_{D_1}(\mathbf{x})$  converges to a Gaussian distribution  $\mathcal{N}(0, \sigma_O^2(\mathbf{x}))$ , with*

$$\sigma_O^2(\mathbf{x}) = \sigma_V^2 \mathbb{E} \left[ \left( h_1^{(1)}(\mathbf{x}) \right)^2 \right]. \quad (6)$$

More generally, one can show that in the limit of infinite width, the process  $u_{D_1}$  is distributed as a centered Gaussian process with kernel

$$K(\mathbf{x}, \mathbf{x}') = \sigma_V^2 \mathbb{E} \left[ h_1^{(1)}(\mathbf{x}) h_1^{(1)}(\mathbf{x}') \right].$$

If we further assume that  $\phi(h_1^{(1)}(\mathbf{x}))$  has a finite second moment, one can prove a similar result for neural networks with multiple hidden layers by induction [14].

2.4.2.  $\alpha$ -stable weights ( $0 < \alpha < 2$ ). We now consider the case that all the weights of the neural network are drawn from an  $\alpha$ -stable distribution with  $\alpha \in (0, 2)$ . As  $D_L$  approaches infinity, we study the convergence of the weighted sum

$$u_{D_L}(\mathbf{x}) = \frac{1}{D_L^{1/\alpha}} \sum_{i=1}^{D_L} V_i^{(L)} h_i^{(L)}(\mathbf{x}), \quad (7)$$

where  $V_i^{(L)}$  satisfies the  $\alpha$ -stable distribution and  $h_i^{(L)}$  is the  $i$ -th node of the last hidden layer defined as

$$h_i^{(L)}(\mathbf{x}) = \phi \left( b_i^{(L-1)} + \sum_{j=1}^{D_{L-1}} V_{ij}^{(L-1)} h_j^{(L-1)}(\mathbf{x}) \right). \quad (8)$$

Note that for a fixed input  $\mathbf{x}$ ,  $\{h_j^{(L)}(\mathbf{x}), V_j^{(L)}\}_{j=1}^{D_{L-1}}$  are pairwise independent and each  $h_i^{(L)}(\mathbf{x})$  follows the same distribution. Thus, we neglect the indices and simply use  $h(\mathbf{x}) := h_i^{(L)}(\mathbf{x})$ . By letting the width of each hidden layer tend to infinity, it is shown in [15] that the final output also converges to an  $\alpha$ -stable distribution. The precise result is stated next.

**Theorem 2.2.** *Assume that all the weights of (7) are i.i.d., and follow an  $\alpha$ -stable distribution with scale parameter  $\gamma$ , where  $\alpha \in (0, 2)$ . Assume also that the activation  $\phi(\cdot)$  satisfies that  $\mathbb{E}[h(\mathbf{x})]^\alpha < \infty$ , where  $h_i^{(L)}(\mathbf{x})$  is defined in (8). Then, as  $D_L \rightarrow \infty$ , the output  $u_{D_L}(\mathbf{x})$  converges in distribution to an  $\alpha$ -stable random variable  $u(\mathbf{x})$  with characteristic function  $\Phi_{u(\mathbf{x})}(t) = \exp(-|\gamma t|^\alpha \mathbb{E}[h(\mathbf{x})]^\alpha)$ .*

We note that the assumption  $\mathbb{E}[h(\mathbf{x})]^\alpha < \infty$  in the theorem always holds for bounded activation functions such as  $\tanh(\cdot)$  and  $\text{sgn}(\cdot)$ .

2.5. **Outputs of neural network priors with finite width.** Since infinite-width neural networks are not practical, we next consider neural network priors with finite width. In particular, we study the distribution of the output's derivative at a fixed point  $\mathbf{x}$ . We distinguish two cases, namely neural networks with heavy-tailed (e.g., Cauchy) weights and with finite moment (e.g., a Gaussian) weights.

We start with the case of a single hidden layer. We first assume that the input is one-dimensional and extend the result to multi-dimensional input later. The network (4) becomes

$$u(x) = \sum_{i=1}^{D_1} V_i^{(1)} \phi \left( b_i^{(0)} + V_i^{(0)} x \right). \quad (9)$$

Assuming  $\phi$  is differentiable, the gradient of  $u(x)$  with respect to  $x$  is

$$u'(x) = \sum_{i=1}^{D_1} V_i^{(1)} V_i^{(0)} \phi'(b_i^{(0)} + V_i^{(0)} x). \quad (10)$$

We now show that the distribution of the derivative (10) is heavy-tailed if the weights from the input to the hidden layer follow a heavy-tailed distribution. A distribution is referred to as heavy-tailed if its tail is heavier than an exponential distribution. The formal definition is given next.

**Definition 2.3.** A random variable  $X$  with cumulative distribution function  $F_X(x)$  is said to be heavy-tailed if

$$\int_{-\infty}^{\infty} e^{t|x|} dF_X(x) = \infty \quad \text{for all } t > 0.$$

To motivate our interest in (10), consider the Taylor expansion of  $u$  at a point  $x$ ,

$$u(x + \delta) - u(x) = u'(x)\delta + o(|\delta|),$$

where  $|\delta|$  is small. When, for fixed  $x$ ,  $u'(x)$  follows a heavy-tailed distribution, the difference  $|u(x + \delta) - u(x)|$  is very large with a non-negligible probability, resulting in a large jump in  $u$ . To study when (10) is heavy-tailed, we first consider  $V_i^{(0)} \phi'(b_i^{(0)} + V_i^{(0)} x)$ . To simplify notation, we neglect indices and introduce the random variable

$$G := V \phi'(B + Vx), \quad (11)$$

which depends on the i.i.d. heavy-tailed and general symmetric random variables  $V$  and  $B$ , respectively. We next show that the distribution of  $G$  is heavy-tailed for appropriate activation functions. Recall that for two measurable spaces  $X, Y$  with  $\mu$  being a measure on  $X$  and a measurable function  $f : X \rightarrow Y$ , the induced measure  $\nu$  on  $Y$  defined by  $\nu(A) = \mu(f^{-1}(A))$ , for any measurable set  $A$ , satisfies

$$\mathbb{E}_{x \sim \mu}(f(x)) = \int_X f(x) \mu(dx) = \int_Y y \nu(dy) = \mathbb{E}_{y \sim \nu} y. \quad (12)$$

The following theorem states the main results.

**Theorem 2.4.** *Assume that in (11),  $V$  follows a symmetric heavy-tailed distribution and  $B$  is a symmetric random variable. Furthermore, assume that  $\phi(\cdot)$  is differentiable and its derivative is bounded away from zero, i.e.,  $|\phi'(\cdot)| \geq c > 0$ . Then the distribution of  $G$  is heavy-tailed.*

*Proof.* We denote the joint cumulative distribution function of  $V$  and  $B$  as  $F_{V,B}(\cdot, \cdot)$ , and the cumulative distribution functions of  $V$  and  $B$  as  $F_V(\cdot)$  and  $F_B(\cdot)$ , respectively. For  $t > 0$ , using (12), we have

$$\begin{aligned} \int_{\mathbb{R}} e^{t|g|} dF_G(g) &= \mathbb{E}_{V,B} \left[ e^{t|V \phi'(B+Vx)|} \right] = \int_{\mathbb{R}} \int_{\mathbb{R}} e^{t|v \phi'(b+vx)|} dF_{V,B}(v, b) \\ &= \int_{\mathbb{R}} \int_{\mathbb{R}} e^{t|v \phi'(b+vx)|} dF_V(v) dF_B(b), \end{aligned}$$



since  $V$  and  $B$  are independent. The boundedness of  $\phi$  from below implies

$$\int_{\mathbb{R}} e^{t|g|} dF_G(g) \geq \int_{\mathbb{R}} \int_{\mathbb{R}} e^{ct|v|} dF_V(v) dF_B(b) \geq \int_{\mathbb{R}} e^{tc|v|} dF_V(v) = \infty,$$

where we used  $\int_{\mathbb{R}} dF_B(b) = 1$  and that  $V$  is heavy-tailed. Thus,  $G$  is heavy-tailed.  $\square$

We note that the assumption of the derivative bounded from below is satisfied for most activation functions including leaky-ReLU and SeLU. Furthermore, we can apply this theorem to more activation functions, e.g.,  $\tanh(\cdot)$ , ReLU, by using  $\tilde{\phi}(x) = \phi(x) + \varepsilon x$ , with small  $\varepsilon > 0$ . Having established that each  $V_i^{(0)} \phi'(b_i^{(0)} + V_i^{(0)} x)$  in (10) is heavy-tailed, we next show that  $u'(x)$  is also heavy-tailed. We first formulate a basic lemma, whose proof can be found in the appendix.

**Lemma 2.5.** *If  $X$  is a heavy-tailed random variable and  $Y$  is an independent symmetric continuous random variable, then we have the following properties:*

- (i) *The product of  $XY$ , is also a heavy-tailed random variable.*
- (ii) *If we further assume that  $Y$  is also heavy-tailed, then the sum of  $X + Y$ , is also a heavy-tailed random variable.*

We now show that all components of the gradient (10) are heavy-tailed under the assumptions in Theorem 2.4. Note that we only require the weights in the last hidden layer to the output to be symmetric continuous random variables. While the result above is for one-dimensional input  $x$ , the generalization to multi-dimensional input  $\mathbf{x}$  by considering the partial derivatives is straightforward. A neural network with multi-dimensional input  $\mathbf{x}$  and one hidden layer is given as

$$u(\mathbf{x}) = \sum_{i=1}^{D_1} V_i^{(1)} \phi \left( b_i^{(0)} + \sum_{j=1}^{D_0} V_{ij}^{(0)} x_j \right). \quad (13)$$

The next theorem extends Theorem 2.4 to networks of the form (13).

**Theorem 2.6.** *Assume  $V_{ij}^{(0)}, b_i^{(0)}$  follow i.i.d. heavy-tailed and symmetric distributions, respectively, and  $V_i^{(1)}$  are i.i.d. symmetric continuous random variables. Further assume that  $\phi(\cdot)$  is differentiable and its derivative is bounded away from zero. Then the partial derivatives of (13),*

$$\partial_{x_k} u(\mathbf{x}) = \sum_{i=1}^{D_1} V_i^{(1)} V_{ik}^{(0)} \phi' \left( b_i^{(0)} + \sum_{j=1}^{D_0} V_{ij}^{(0)} x_j \right) \quad (14)$$

*are also heavy-tailed.*

The proof follows by using that each component is heavy-tailed. Next, we prove our main theorem for neural networks with multiple hidden layers and weights from heavy-tailed and finite-moments distributions.

**Theorem 2.7.** *Assume the neural network (4) and that  $\mathbf{b}^{(l)}$  are symmetric random variables for  $l = 0, \dots, L - 1$ . Furthermore, assume that  $\phi(\cdot)$  is differentiable, and its derivative is bounded and bounded away from zero. Then, for a fixed  $\mathbf{x}$ , the distribution of  $\partial_{x_k} u(\mathbf{x})$  satisfies:*

- (i) *If the weights in  $\mathbf{V}^{(l)}$  are i.i.d. symmetric heavy-tailed and  $\mathbf{V}^{(L)}$  are i.i.d. symmetric continuous random variables, then all  $\partial_{x_k} u(\mathbf{x})$  are heavy-tailed.*

(ii) If  $\mathbf{V}^{(l)}$  are i.i.d. symmetric random variables of finite  $k$ -th order moment, then all  $\partial_{x_k} u(\mathbf{x})$  have finite moment of  $k$ -th order.

*Proof.* We use induction for the proof. The partial derivative is

$$\partial_{x_k} u(\mathbf{x}) = \sum_{i=1}^{D_L} V_i^{(L)} \phi' \left( b_i^{(L-1)} + \sum_{j=1}^{D_{L-1}} V_{ij}^{(L-1)} h_j^{(L-1)}(\mathbf{x}) \right) \left( \sum_{j=1}^{D_{L-1}} V_{ij}^{(L-1)} \partial_{x_k} h_j^{(L-1)}(\mathbf{x}) \right), \quad (15)$$

where  $\partial_{x_k} h_j^{(L-1)}(\mathbf{x})$  is the partial derivative of the  $j$ -th component of the  $(L-1)$ -th hidden layer.

We consider first case (i). In Theorem 2.6, for one hidden layer, we have shown that the distribution of the partial derivative is heavy-tailed. We assume that this argument holds for neural networks with  $L-1$  hidden layers. It is easy to see that

$$\sum_{j=1}^{D_{L-1}} V_{ij}^{(L-1)} \partial_{x_k} h_j^{(L-1)}(\mathbf{x}) \quad (16)$$

is also heavy-tailed using Lemma 2.5 and since each component is the partial derivative of the output of a neural network of  $L-1$  hidden layers and  $\cdot$ . Since  $\phi'(\cdot)$  is bounded away from zero,  $V_i^{(L)} \phi' \left( b_i^{(L-1)} + \sum_{j=1}^{D_{L-1}} V_{ij}^{(L-1)} h_j^{(L-1)}(\mathbf{x}) \right)$  is heavy-tailed following the proof in Theorem 2.4, and thus that (15) is also heavy-tailed by Lemma 2.5.

For case (ii), we start with a one-hidden-layer neural network given by

$$u(\mathbf{x}) = \sum_{i=1}^{D_1} V_i^{(1)} \phi \left( b_i^{(0)} + \sum_{j=1}^{D_0} V_{ij}^{(0)} x_j \right), \quad (17)$$

with corresponding partial derivative

$$\partial_{x_k} u(\mathbf{x}) = \sum_{i=1}^{D_1} V_i^{(1)} V_{ij}^{(0)} \phi' \left( b_i^{(0)} + \sum_{j=1}^{D_0} V_{ij}^{(0)} x_j \right).$$

Note that  $|\phi'(\cdot)|$  is bounded by the assumption. Therefore, the partial derivative of the output has finite  $k$ -th moment since  $V_i^{(1)}, V_{ij}^{(0)}$  are i.i.d. random variables of finite  $k$ -th moment. We now assume that the result holds for any neural network with  $L-1$  hidden layers. Then (16) has finite  $k$ -th moment since both  $V_{ij}^{(L-1)}$  and  $\partial_{x_k} h_j^{(L-1)}(\mathbf{x})$  have finite  $k$ -th moment and are independent of each other. This implies that the partial derivative in (15) also has finite  $k$ -th moment. Thus, the result follows by induction.  $\square$

Again, note that the results in this section hold for heavy-tailed weights, which includes  $\alpha$ -stable weights. From Theorem 2.7, one can see that the derivative of the neural network output with Gaussian weights has finite moments, which implies smooth outputs in practice. In contrast, the derivative of the neural network output is heavy-tailed if all the weights before the last hidden layer are  $\alpha$ -stable distributed,  $0 < \alpha < 2$ . This implies that the derivative of the output can have extreme values with non-negligible probability and thus the corresponding neural network outputs can have large jumps, emulating discontinuities even when the activation function is smooth. Furthermore, we only assume the weights before the last hidden layer to be  $\alpha$ -stable. Biases can follow any symmetric random distribution. For the numerical

experiments in Sec. 4, we study one type of such neural network priors, which has Cauchy random variables as the weights except for the last hidden layer, which has Gaussian weights. We refer to this setup as the Cauchy-Gaussian prior.

**3. Bayesian inference with neural network priors.** In this section, we study Bayesian inverse problems in function space with neural network priors. We first use observation data to define the posterior on the weights. Several approaches to probe the posterior distribution are then discussed, including maximum a posterior (MAP) estimation via optimization, and Markov chain Monte Carlo (MCMC) sampling.

In the Bayesian approach, one treats the inverse problem as statistical inference of the function  $u$  in a function space  $\mathcal{U}$ . This amounts to finding the posterior distribution of  $u$  that reflects the prior information and the observations. The forward map is the parameter-to-observable operator  $\mathcal{F} : \mathcal{U} \rightarrow \mathbb{R}^{N_{\text{obs}}}$  that maps the parameter field  $u$  to observations in  $\mathbb{R}^{N_{\text{obs}}}$ , where  $N_{\text{obs}}$  is the dimension of the observables. We assume additive Gaussian errors  $\varepsilon \sim \mathcal{N}(0, \eta^2 I_{N_{\text{obs}}})$ , so that the observations are

$$\mathbf{y}_{\text{obs}} = \mathcal{F}(u) + \varepsilon. \tag{18}$$

Hence, the likelihood for given  $u$  is

$$p(\mathbf{y}_{\text{obs}}|u) \propto \exp\left(-\frac{1}{2\eta^2} \|\mathcal{F}(u) - \mathbf{y}_{\text{obs}}\|_2^2\right).$$

Given a prior measure  $\mu^0$ , the posterior measure  $\mu^y$  of  $u$  is defined via Bayes' rule

$$\frac{d\mu^y}{d\mu^0} = \frac{1}{Z} p(\mathbf{y}_{\text{obs}}|u), \tag{19}$$

where the left-hand side is the Radon–Nikodym derivative of the posterior measure  $\mu^y$  with respect to the prior measure  $\mu^0$  and  $Z = \int_{\mathcal{U}} p(\mathbf{y}_{\text{obs}}|u) d\mu_0$  is the normalization constant.

Note that in infinite dimensions, Bayes' formula cannot be written in terms of probability density functions since there is no Lebesgue measure against which to define the densities of the prior and posterior distributions. Thus, finite-dimensional approximations of the prior and posterior distributions are proposed in [5, 11]. In particular, we assume that the prior distribution is approximated by a finite-dimensional measure  $\mu^{0,h}$  which is absolutely continuous with respect to the Lebesgue measure  $\lambda$ ; the resulting posterior  $\mu^{y,h}$  is then also absolutely continuous with respect to  $\lambda$ . If we define  $p_{\text{post}}(u|\mathbf{y}_{\text{obs}})$  and  $p_{\text{prior}}(u)$  as the Lebesgue densities of  $\mu^{0,h}$  and  $\mu^{y,h}$ , respectively, we have

$$p_{\text{post}}(u|\mathbf{y}_{\text{obs}}) = \frac{d\mu^{y,h}}{d\lambda} = \frac{d\mu^{y,h}}{d\mu^{0,h}} \frac{d\mu^{0,h}}{d\lambda} \propto p(\mathbf{y}_{\text{obs}}|u)p_{\text{prior}}(u). \tag{20}$$

In this paper, we estimate  $u$  defined by the the finite-dimensional network parameterization. The output of the neural network is a function of the weights, which we denote by  $u = \Psi(\mathbf{w})$ , where  $\mathbf{w}$  represents the weights inside the neural network. This connects the weights  $\mathbf{w}$  with the observations  $\mathbf{y}_{\text{obs}}$  as

$$\mathbf{y}_{\text{obs}} = \mathcal{F}(\Psi(\mathbf{w})) + \varepsilon.$$

This allows one to infer  $u$  by learning the posterior distribution on the weights of the neural network instead. Again, the posterior measure  $\mu_w^y$  on the weights can be

computed by Bayes’ rule as

$$\frac{d\mu_w^y}{d\mu_w^0} \propto p(\mathbf{y}_{\text{obs}}|\mathbf{w}), \quad (21)$$

where  $p(\mathbf{y}_{\text{obs}}|\mathbf{w})$  is the likelihood for given weights  $\mathbf{w}$ . The finite-dimensional equation (21) can be expressed in terms of densities. For the prior density on  $\mathbf{w}$ , we use the product of one-dimensional densities on each component.

**3.1. Posterior approximation based on minimizers.** Here, we give an overview of methods that approximate the posterior distribution using optimization. Minimization-based point estimation only provides limited uncertainty information, but it is computationally much cheaper than sampling, which we discuss in Sec. 3.2.

**3.1.1. MAP estimation.** A widely-used estimation of the posterior (21) is maximum a posteriori (MAP) estimation. MAP estimates  $\mathbf{w}_{\text{map}}$  are obtained by maximizing the posterior distribution  $p_{\text{post}}(\mathbf{w}|\mathbf{y}_{\text{obs}})$ :

$$\mathbf{w}_{\text{map}} = \arg \max_{\mathbf{w}} p_{\text{post}}(\mathbf{w}|\mathbf{y}_{\text{obs}}).$$

This is equivalent to

$$\mathbf{w}_{\text{map}} = \arg \min_{\mathbf{w}} J(\mathbf{w}) := \frac{1}{2\eta^2} \|\mathcal{F}(\Psi(\mathbf{w})) - \mathbf{y}_{\text{obs}}\|_2^2 + R(\mathbf{w}), \quad (22)$$

where  $R(\mathbf{w}) := -\log(p_{\text{prior}}(\mathbf{w}))$  is the regularization term. We assume that the prior on  $\mathbf{w}$  is an  $\alpha$ -stable distribution. Note that (22) is a non-convex optimization problem due to the presence of the neural network and due to a possibly non-linear map  $\mathcal{F}$ . It is thus not guaranteed (and even unlikely) that we find the global minimum numerically. Instead, we likely find a local minimizer, which we denote by  $\mathbf{w}_{\text{loc}}$ . Which local minimizer is found may depend on the initialization of the optimization algorithm and the algorithm itself. We will use local minima to construct different approximations to the posterior distribution as discussed next.

**3.1.2. Laplace approximation.** Based on a local minimum  $\mathbf{w}_{\text{loc}}$ , the Laplace approximation is defined as the Gaussian distribution

$$\mathcal{N}(\mathbf{w}_{\text{loc}}, \nabla^2 J(\mathbf{w}_{\text{loc}})^{-1}), \quad (23)$$

where  $\nabla^2 J(\mathbf{w}_{\text{loc}})$  denotes the Hessian of the objective function (22) at the local minimum  $\mathbf{w}_{\text{loc}}$ , assuming that it is positive definite. That is, the Laplace approximation replaces the true posterior using a Gaussian distribution centered at the  $\mathbf{w}_{\text{loc}}$  with ‘local’ covariance information of the posterior distribution [5, 32]. The Laplace approximation coincides with the true posterior if the mapping  $\mathbf{w} \mapsto \mathcal{F}(\Psi(\mathbf{w}))$  is linear and the prior and observation error distributions are Gaussian. The approximation might be insufficient when the posterior distribution is multimodal or heavy-tailed. As reported in [20], we observed numerically that the Laplace approximation can lead to substantial overestimation of the variance, and hence we do not consider it further in this paper.

3.1.3. *Ensemble method.* A heuristic approach to estimate uncertainty is based on the set of local minima computed with different initializations. This approach is known as the ensemble method or model averaging method [29]. Local minimizers are averaged to approximate the posterior mean and the variation of minimizers is used to estimate uncertainty. Although not well understood theoretically, the ensemble method can provide useful and cheap uncertainty quantification compared to more sophisticated approaches [23, 36]. We will show results obtained with this heuristic approach as part of our numerical results.

3.1.4. *Last-layer Gaussian regression.* This approach starts with finding a minimizer for networks where the last layer is Gaussian. The output of the neural network (4) can be viewed as a linear combination of the nodes in the last hidden layer. For linear parameter-to-observable maps  $\mathcal{F}(\cdot)$  and Gaussian weights between the last hidden layer to the output, (4) reduces to a Gaussian regression problem upon fixing the weights in all previous layers. This is related to the majority voting algorithm [23] except that here we use it to quantify uncertainty. The output function can be represented as

$$u(\mathbf{x}) = \sum_{j=1}^{D_L} \nu_j f_j(\mathbf{x}) = \mathbf{f}(\mathbf{x})^T \boldsymbol{\nu},$$

where  $D_L$  denotes the width of the last hidden layer, i.e., the number of base functions,  $\mathbf{f}(\mathbf{x}) = [f_1(\mathbf{x}), \dots, f_{D_L}(\mathbf{x})]^T$  denotes the vector containing the base functions, and  $\boldsymbol{\nu} = [\nu_1, \dots, \nu_{D_L}]^T$  is the weight vector, which follows a multivariate Gaussian prior  $\mathcal{N}(0, \frac{1}{D_L} I_{D_L})$ . Thus, the forward model is  $\mathbf{y}_{\text{obs}} = \mathcal{F}\mathbf{f}(\cdot)^T \boldsymbol{\nu} + \boldsymbol{\varepsilon} = \mathbf{F}^T \boldsymbol{\nu} + \boldsymbol{\varepsilon}$ , where  $\mathbf{F} = [\mathcal{F}f_1, \dots, \mathcal{F}f_{D_L}]^T$  and  $\mathcal{F}(\cdot)$  is the linear parameter-to-observable mapping. By Bayes' formula, the posterior distribution of  $\boldsymbol{\nu}$  follows a multivariate Gaussian distribution  $\mathcal{N}(\boldsymbol{\nu}_n, \Sigma_n)$  with

$$\boldsymbol{\nu}_n = \frac{1}{\eta^2} \Sigma_n \mathbf{F}^* \mathbf{y}_{\text{obs}}, \quad \Sigma_n^{-1} = \frac{1}{\eta^2} \mathbf{F}^* \mathbf{F} + I_{D_L},$$

where  $\mathbf{F}^*$  is the conjugate transpose of  $\mathbf{F}$ .

Note that this Gaussian distribution is  $D_L$ -dimensional, which is much smaller than the number of weights. The covariance  $\Sigma_n$  can thus be computed and factored easily to generate samples. The base functions  $f_i$ , which are found through optimization, typically contain local structural information such as jumps, and so the  $f_i$  essentially provide a basis adapted to the inverse problem [6]. The assumption of a linear parameter-to-observable mapping  $\mathcal{F}$  is restrictive. However, when  $\mathcal{F}$  is nonlinear this approach may still provide a form of dimension reduction for use with other sampling/approximation methods.

3.2. **Posterior approximation using MCMC sampling.** Sampling methods aim at full exploration of the posterior distribution. MCMC explores the posterior distribution  $p(\mathbf{w}|\mathbf{y}_{\text{obs}})$  by constructing a Markov chain which targets the posterior in stationarity; states of this chain then form a sequence of correlated samples following convergence. One starts with an initial state  $\mathbf{w}^{(0)}$  and proposes another state based on a Markov transition kernel. This proposed state is then accepted or rejected based on an acceptance criterion. Iterating this procedure is the basis for generating a sequence of MCMC samples.

Ideally one desires the correlation between states of the chain to be minimal in order to reduce the cost of computing accurate uncertainty estimates: generating

each proposal and/or acceptance probability typically involves evaluation of the likelihood function and possibly its derivatives. Many classical MCMC algorithms suffer from increasing correlations between samples when the dimension of the parameter space is increased, which is an issue in settings such as ours where the number of weights to be inferred is high [19]. A simple MCMC method which does not suffer from this dimensional dependence, in the case of a Gaussian prior, is the preconditioned Crank-Nicolson (pCN) method [12]. In this method the proposed states encode the prior information via a rescaling and random perturbation of the current state, and the acceptance probability requires only evaluation of the likelihood; see [12] for a full statement of the algorithm. In this algorithm one must choose a scalar parameter  $\beta$  that controls the size of the perturbation in proposed states: if the perturbations are too large, proposed states will be unlikely to be accepted, but if they are too small the states of the chain will be highly correlated, and so a balance must be achieved. In practice this parameter may be adapted on-the-fly to ensure a certain proportion of proposals are accepted. Variants of pCN are available that use gradient and curvature information of the likelihood in order to generate more feasible proposals with larger perturbations, reducing correlation between samples in exchange for increased computational cost per sample; see [3] for a review. In this paper we will use only the pCN method.

We remark that our prior is in general non-Gaussian, however we may still utilize the above methods via a reparameterization typically known as non-centering [10]: we rewrite our prior as a nonlinear transformation of a Gaussian distribution. Since our prior is assumed to be an independent product of one-dimensional distributions this mapping may be found using the inverse CDF method. For example, in the case of a standard Cauchy prior we define the mapping

$$\Lambda(p) = \tan \left[ \pi \left( \psi_G(p) - \frac{1}{2} \right) \right],$$

where  $\psi_G$  is the standard Gaussian cumulative density function: if  $p \sim N(0, 1)$ ,  $\Lambda(p)$  is then a standard Cauchy sample. We therefore compose our likelihood function with  $\Lambda$  acting componentwise, and apply the pCN method assuming independent  $N(0, 1)$  priors on each weight. Transforming the resulting MCMC samples with the function  $\Lambda$  componentwise then provides samples from our desired posterior.

**4. Numerical experiments.** In this section, we study the behavior of neural network priors for Bayesian inverse problems. Our goal is to compare inversion results obtained with neural network priors with Cauchy and Gaussian weight distributions. For that purpose, we use deconvolution problems in one and two dimensions. All numerical experiments are implemented using the PyTorch 1.9.0 environment.

#### 4.1. One-dimensional deconvolution.

**Problem 1.** *We first consider a deconvolution problem on the interval  $\mathcal{D} = [-1, 1]$  with forward model*

$$\mathbf{y}_{obs} = A(u) + \varepsilon, \quad \varepsilon \sim \mathcal{N}(0, \eta^2 I_{N_{obs}}),$$

where  $u$  is the unknown, potentially discontinuous parameter to be recovered. The forward operator is defined as  $A = P \circ B$ , where  $B : L^\infty(\mathcal{D}) \rightarrow \mathcal{C}^\infty$  denotes the blurring operator defined by the convolution with a mean-zero Gaussian kernel with variance  $0.03^2$ , and  $P : \mathcal{C}^\infty \rightarrow \mathbb{R}^{N_{obs}}$  is the evaluation operator at  $N_{obs} = 50$

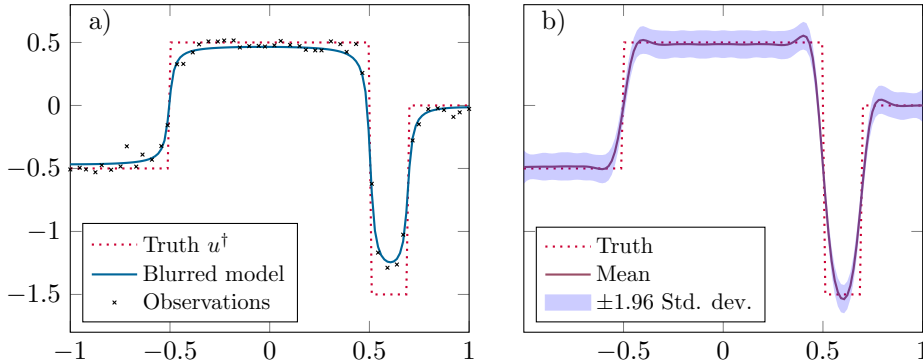


FIGURE 3. Setup for Problem 1. Shown in (a) are the truth model and synthetic observations. As reference, shown in (b) is the result of Gaussian process regression with the covariance operator  $0.25(I - 10\Delta)^{-2}$ .

uniformly distributed points. The variance of the errors  $\varepsilon$  is  $\eta^2 = 0.05^2$ . We discretize the forward operator using a uniform mesh with 128 points.

The true model and the synthetic observations are shown in Figure 3(a). As a reference, we show the reconstruction obtained with a Gaussian process regression in Figure 3(b). Here, we used a mean-zero Gaussian process prior with the Matérn covariance operator  $0.25(I - 10\Delta)^{-2}$  with homogeneous Neumann boundary conditions. Here and in the remainder of this section, we show an uncertainty region corresponding to the 95% credible interval. For Gaussians, this corresponds to  $\hat{\mu} \pm 1.96\hat{\sigma}$ , where  $\hat{\mu}$  and  $\hat{\sigma}$  denote the sample mean and sample pointwise standard deviation, respectively. For the following neural network priors, we use a network with 3 hidden layers with widths [50, 50, 100].

4.1.1. *Optimization-based methods.* For the optimization-based methods, the objective function to be minimized is

$$J(\mathbf{w}) = \frac{1}{2\eta^2} \|A(\Psi(\mathbf{w})) - \mathbf{y}_{\text{obs}}\|_2^2 + R(\mathbf{w}). \quad (24)$$

For Gaussian weights, the regularization  $R(\mathbf{w})$  is  $R_G(\mathbf{w})$  and for Cauchy weights it is  $R_C(\mathbf{w})$ , defined as

$$R_G(\mathbf{w}) := \frac{1}{2} \sum_i w_i^2, \quad R_C(\mathbf{w}) := \sum_i \log(1 + w_i^2), \quad (25)$$

where the summation is over all weights  $\mathbf{w}$ . We compare reconstructions for three regularizations, namely:

- (i) Fully Gaussian weights,
- (ii) Cauchy-Gaussian weights, i.e., all weights except those in the last layer follow a Cauchy distribution. The weights in the last layer are Gaussian,
- (iii) Fully Cauchy weights.

For each optimization, we first use 500 iterations of the Adaptive Moment Estimation (Adam) method, which adaptively changes the stepsize. Following that, we use 1500 iterations using the Limited-memory Broyden–Fletcher–Goldfarb–Shannon (LBFGS) algorithm [28] for a faster convergence to a local minimum. Examples of

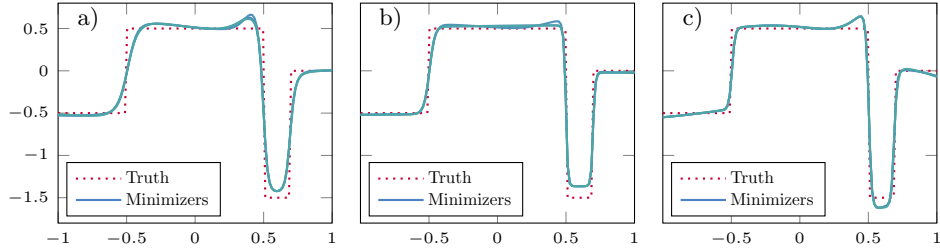


FIGURE 4. Shown are reconstructions using different initializations obtained through optimization for Problem 1. The results correspond to the Gaussian (a), Cauchy-Gaussian (b), and fully Cauchy (c) weights.

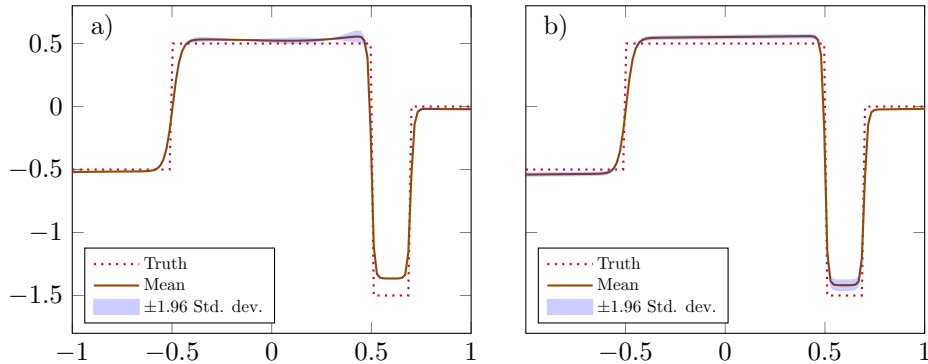


FIGURE 5. Shown are the means and pointwise standard deviations obtained with the ensemble method (a) and the last-layer Gaussian regression method (b). Both results are for Cauchy-Gaussian priors for Problem 1.

reconstructions of the parameter function  $u$  for the different regularizations are shown in Figure 4. We observe that while optimizations from different initializations typically result in different weights, the differences in the outputs  $u$  are small. Moreover, the reconstructions using Gaussian regularizations are smooth while the reconstructions with Cauchy regularizations capture the discontinuities in the parameter function better, although overall the differences are rather small.

We also study the uncertainty based on these reconstructions obtained with the ensemble method (Sec. 3.1.3) and the last-layer Gaussian regression method (Sec. 3.1.4). The results obtained with both approaches for Cauchy-Gaussian weights are shown in Figure 5. A quantitative summary of these results using the ensemble method is shown in Table 1. Here, we report the quantities  $\|\mathbb{E}[u] - u^\dagger\|_{L^1} / \|u^\dagger\|_{L^1}$  and the mean and standard deviation of  $\|u - u^\dagger\|_{L^1} / \|u^\dagger\|_{L^1}$ , where  $u^\dagger$  and  $u$  denote the truth and reconstructions, respectively. Based on the numerical reconstructions and the  $L^1$  relative error, we observe that the results obtained with Cauchy-Gaussian and fully Cauchy weights better fit the discontinuities of the truth parameter better.



TABLE 1. Relative  $L^1$ -error of reconstructions obtained using the ensemble method with Gaussian, Cauchy-Gaussian and Cauchy priors in Problem 1.

Regularizations	Gaussian	Cauchy-Gaussian	Cauchy
$\ \mathbb{E}[u] - u^\dagger\ _{L^1} / \ u^\dagger\ _{L^1}$	8.35	5.90	5.53
$\mathbb{E}[\ u - u^\dagger\ _{L^1}] / \ u^\dagger\ _{L^1}$	8.44	5.91	5.56
$\text{Std}[\ u - u^\dagger\ _{L^1}] / \ u^\dagger\ _{L^1}$	0.10	0.11	0.13

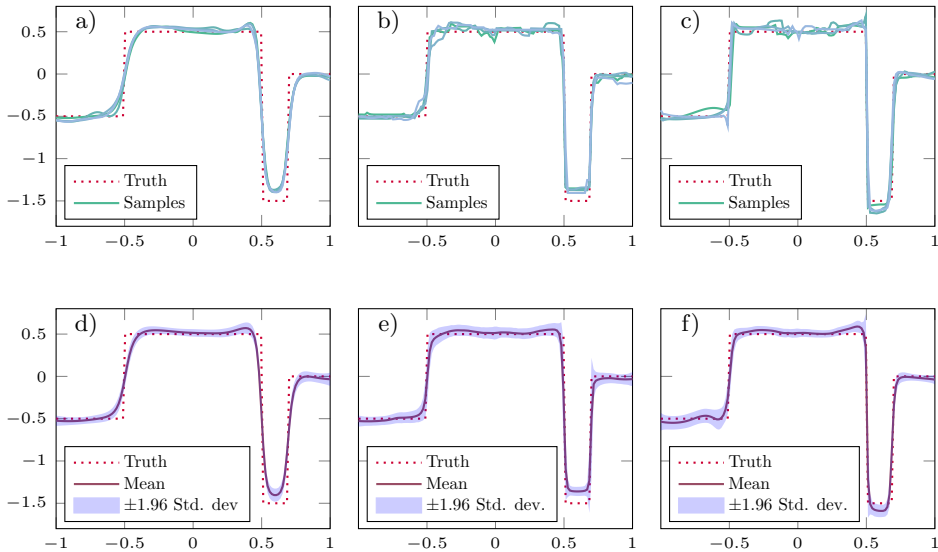


FIGURE 6. Shown in (a,b,c) are samples and in (d,e,f) the uncertainty of posterior distributions with different neural network priors for Problem 1. The plots correspond to the Gaussian (a,d), Cauchy-Gaussian (b,e), and Cauchy (c,f) neural network priors.

4.1.2. *MCMC sampling.* We also aim at exploring the posterior using the MCMC method. We use a local minimum obtained with the optimization method as the starting point to reduce the burn-in phase. The pCN method is used to generate  $5 \times 10^6$  samples as discussed in Sec. 3.2. We use an adaptive method to adjust the value of  $\beta$  to maintain an acceptance rate of about 30%. Note that we always use Gaussian increments in the pCN method. Numerical results obtained with each neural network prior are shown in Figure 6. We observe that the pCN samples based on Cauchy weights capture the discontinuities better. The sample mean and uncertainty region indicate a better fit to the truth model when we use the Cauchy-Gaussian or the Cauchy neural network prior. We also compare the  $L^1$  relative error between the truth  $u^\dagger$  and the samples  $u$  generated using each prior in Table 2. Note that the landscape of the posterior is multi-modal due to the nonlinearity of the neural network priors. Thus, these results might not fully explore the posterior distribution but only provide a local estimate of the uncertainty around one (or several) local minimizers.

## 4.2. Two-dimensional deconvolution.

TABLE 2. Relative  $L^1$ -error of samples computed by pCN with Gaussian, Cauchy-Gaussian and Cauchy priors in Problem 1.

Neural network prior	Gaussian	Cauchy-Gaussian	Cauchy
$\ \mathbb{E}[u] - u^\dagger\ _{L^1} / \ u^\dagger\ _{L^1}$	8.14	5.66	4.74
$\mathbb{E}[\ u - u^\dagger\ _{L^1}] / \ u^\dagger\ _{L^1}$	8.57	6.45	5.63
$\text{Std}[\ u - u^\dagger\ _{L^1}] / \ u^\dagger\ _{L^1}$	0.63	0.57	0.73

**Problem 2.** This is a two-dimensional deblurring problem on  $\mathcal{D} = [-1, 1]^2$ . The forward model involves a PDE-solve, namely the solution of

$$(I - \kappa\Delta)y = u \quad \text{in } \mathcal{D}, \quad (26a)$$

$$\frac{\partial y}{\partial n} = 0 \quad \text{on } \partial\mathcal{D}, \quad (26b)$$

where  $y$  and  $u$  are PDE solution and the unknown parameter field, respectively. In (26),  $\kappa = 0.01$ , which controls the amount of blurring. The forward model is denoted as

$$\mathbf{y}_{obs} = A(u) + \varepsilon, \quad \varepsilon \sim \mathcal{N}(0, \eta^2 I_{N_{obs}}),$$

where  $\eta = 0.01$  and the forward operator is  $A = P \circ B$ . Here,  $B : L^{infty}(\mathcal{D}) \rightarrow \mathcal{C}^\infty$  is the PDE operator and  $P : \mathcal{C}^\infty \rightarrow \mathbb{R}_{obs}^N$  point evaluation on a uniform grid of  $14 \times 14$  points. We discretize the forward PDE on a uniform mesh of  $100 \times 100$  grid points using the standard 5-point finite difference stencil.

The true parameter function  $u^\dagger$  and the blurred model are shown in Figure 7. Similar to Problem 1, we test the optimization and pCN methods on this problem with different neural network priors. For all tests, we use the three-hidden-layer neural network structure with layer widths of  $[80, 80, 1000]$ . Note that the input dimension of the neural network is 2, and the output dimension is 1. This example is computationally more costly than Problem 1 due to the required PDE solves and the use of a wider network. Since the PDE solve requires most of the computation time, we use an upfront Cholesky decomposition of the discretized blurring operator to accelerate the computation.

4.2.1. *Optimization-based methods.* The objective to be minimized is formally as in the one-dimensional case. We use the Adam method for the first 200 steps followed by 1500 iterations of L-BFGS. The initial step size is set to be 0.01 for each method. Reconstructions obtained with different regularizations and different initialization in the optimization are shown in Figure 7. We observe that the reconstructions using the Cauchy neural network capture the edges better, especially the middle edge and the right bottom block. In contrast, the fully Gaussian neural network tends to result in smooth reconstructions. We also note that the fully Cauchy neural network results in better reconstructions of the linear ramp in the upper part of the image compared to the Cauchy-Gaussian neural network.

We also study the uncertainty using the ensemble method from Sec. 3.1.3. Results for different regularizations are shown in Figure 8. We observe that the Cauchy-Gaussian neural network outperforms the Gaussian neural network for edge detection.

An alternative uncertainty quantification approximation method is the last-layer Gaussian regression based on the trained neural network (Sec. 3.1.4). The mean and

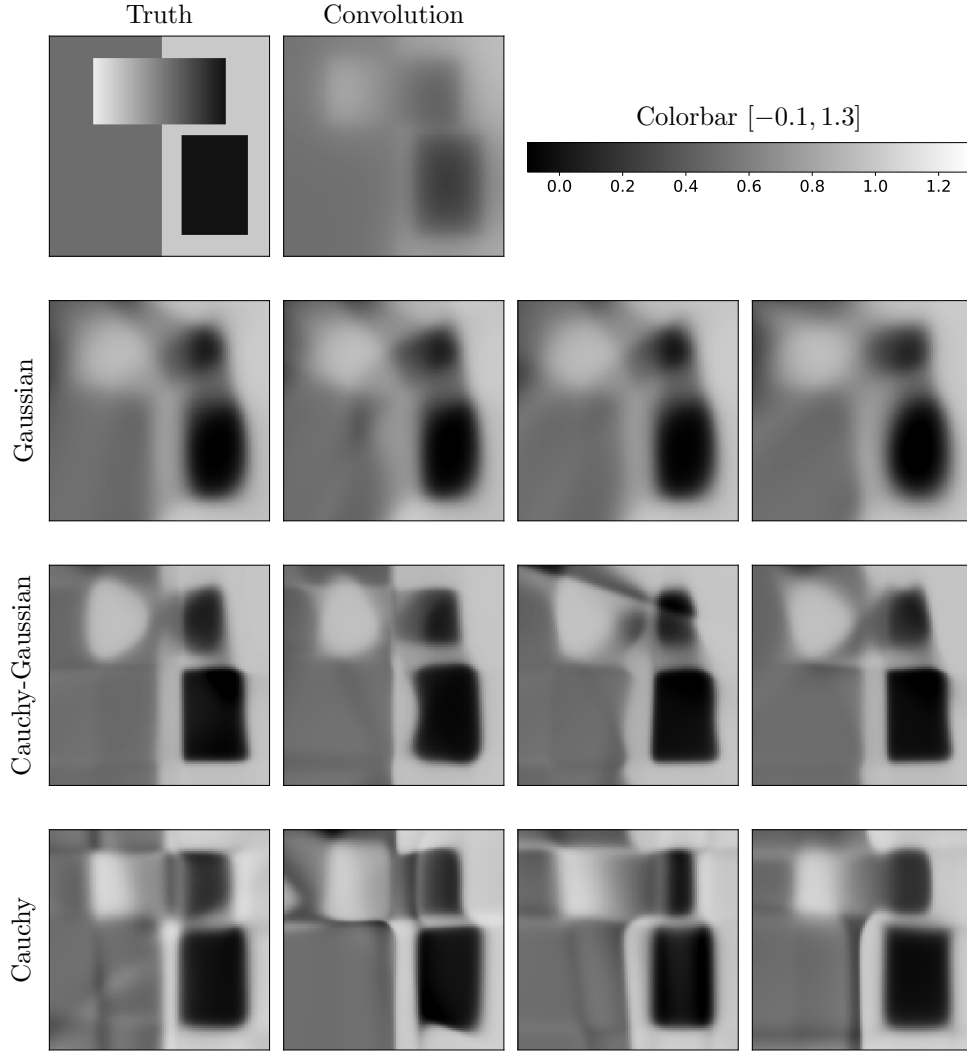


FIGURE 7. Shown in the first row are the truth  $u^\dagger$  and blurred models used for Problem 2. We show minimizers obtained using the optimization method with different initializations. Results are shown for Gaussian weights (second row), Cauchy-Gaussian weights (third row), and Cauchy weights (forth row).

standard deviation obtained by this approach from a fully Gaussian and a Cauchy-Gaussian neural network are shown in Figure 9. Since the mean of the Gaussian regression is identical to the reconstruction we exploit, we only show the standard deviation of each neural network with different regularizations.

4.2.2. *MCMC sampling.* We also test the MCMC sampling method on this two-dimensional deconvolution example using  $10^6$  samples of the adaptive pCN method. A numerical comparison of the uncertainty with different priors is shown in Figure 10. We observe that the mean of the chain with a Cauchy neural network

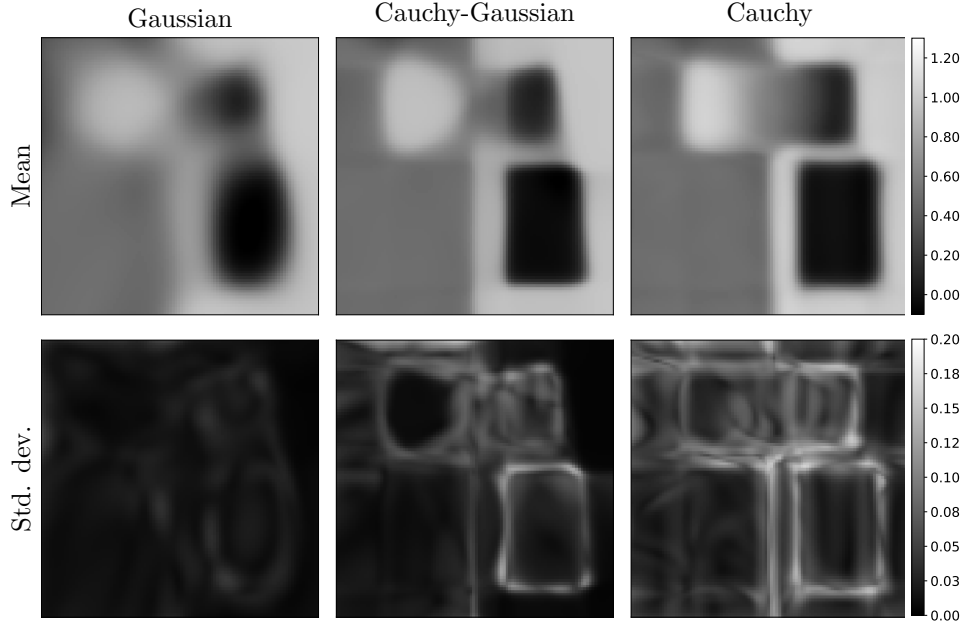


FIGURE 8. Results obtained with ensemble method for Problem 2. Shown are the ensemble means (top row) and standard deviation (bottom row) obtained with Gaussian weights (left), Cauchy-Gaussian weights (middle), and fully Cauchy weights (right).

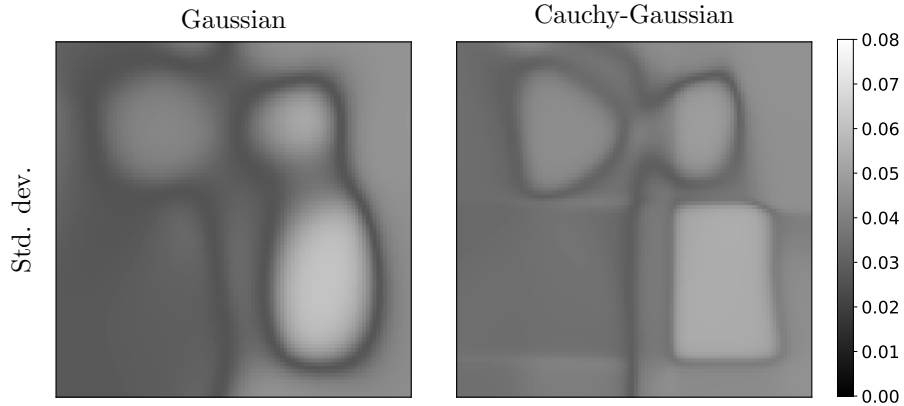


FIGURE 9. Results for last-layer Gaussian regression, Problem 2. Shown are the standard deviations with last-layer base functions from a pre-trained network. The figures are for networks with Gaussian (left) and Cauchy-Gaussian (right) weights.

prior recovers the edges of the parameter function better while the Gaussian neural network prior results in smoother reconstructions. From the plots of the standard deviation, we also note that the result obtained with a Cauchy neural network prior

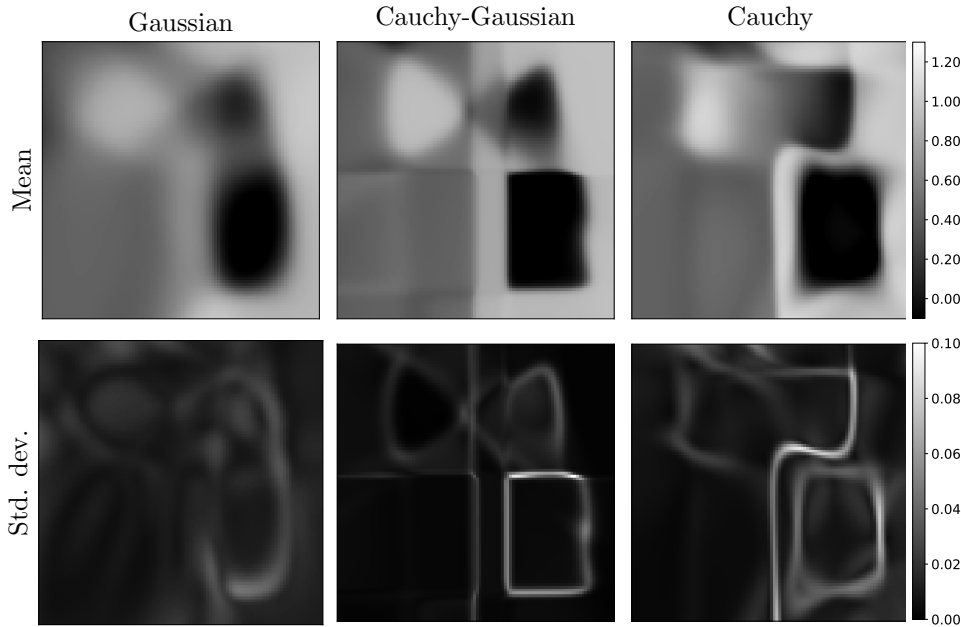


FIGURE 10. MCMC sampling results for Problem 2. Shown are the means (top row) and standard deviations (bottom row) for neural network priors with Gaussian weights (left), Cauchy-Gaussian weights (middle), and fully Cauchy weights (right).

possesses a larger variation around the edges compared to other regions, which implies a better edge detection. We also note that the neural network priors with fully Cauchy weights can learn the linearly-changing block on the top better than the Cauchy-Gaussian network prior.

**5. Summary and conclusions.** The main target of this work is to study neural network priors for infinite-dimensional Bayesian inverse problems. Samples of these priors are outputs of neural networks with random weights from different distributions. Theoretically, we study finite-width neural networks with  $\alpha$ -stable weights, and show that the derivative of the output at a fixed point is heavy-tailed for Cauchy weights. We also present a numerical comparison of Cauchy and Gaussian neural networks priors in Bayesian inverse problems. We conclude that: (1) Neural network priors are able to capture discontinuities and they are discretization-independent by design. Conditioning these priors with observations can require many hundreds of evaluations of the network and the forward map to compute point approximations of the posterior. Attempting sampling of the posterior distribution requires tens of thousands of network and forward map evaluations. (2) Not unexpectedly, the optimization landscapes for optimization with Bayesian neural networks have multiple local minima even if the forward map is linear as in the deblurring examples we study. (3) We observe that upon optimization, most weights of Cauchy neural networks are close to zero at (local) minimizers. Optimized Cauchy networks thus have substantial sparsity, which is a consequence of the regularization resulting from the Cauchy density. (4) While we only focused on fully connected networks, one could

use block-diagonal weight matrices, thus requiring substantially fewer weights. We found in numerical experiments (which are not shown here) that for Cauchy weights, the resulting distributions for the output do not differ much between block diagonal and fully connected networks.

**Appendix A. Proof of Lemma 2.5.** For convenience, we present a compact proof for this lemma, starting with the first part (i). The sequence

$$a_N(t) := \int_{-N}^N e^{t|x|} f_X(x) dx,$$

is increasing with respect to  $N$  and  $t$  and converges to infinity as  $N \rightarrow \infty$  for any given  $t > 0$  by definition of heavy-tailed distributions. Since  $Y$  is symmetric, one can find an interval  $[a, b]$ ,  $0 < a < b$ , in which  $f_Y(y) \geq \varepsilon > 0$ . The density function of  $Z = XY$  is given by [31, p. 141]

$$f_Z(z) = \int_{-\infty}^{\infty} f_X\left(\frac{z}{y}\right) f_Y(y) \frac{1}{|y|} dy.$$

Thus for any  $t > 0$  we have, using a change of variables and Fubini's theorem,

$$\begin{aligned} \int_{-N}^N e^{t|z|} f_Z(z) dz &= \int_{-N}^N e^{t|z|} \int_{-\infty}^{\infty} f_X\left(\frac{z}{y}\right) f_Y(y) \frac{1}{|y|} dy dz \\ &= \int_{-\infty}^{\infty} f_Y(y) \frac{y}{|y|} \left( \int_{-N/y}^{N/y} e^{t|yx|} f_X(x) dx \right) dy \\ &= 2 \int_0^{\infty} f_Y(y) \left( \int_{-N/y}^{N/y} e^{t|yx|} f_X(x) dx \right) dy \\ &= 2 \int_0^{\infty} f_Y(y) a_{N/y}(ty) dy \geq 2\varepsilon a_{N/b}(ta)(b-a), \end{aligned}$$

which approaches infinity as  $N \rightarrow \infty$ , which gives the result.

For part (ii) of the lemma, since  $Y$  is heavy-tailed, for any  $t > 0$  at least one of the integrals  $\int_{-\infty}^0 e^{-ty} f_Y(y) dy$  or  $\int_0^{\infty} e^{ty} f_Y(y) dy$  is infinite. Without loss of generality, we assume  $\int_0^{\infty} e^{ty} f_Y(y) dy = \infty$ . Then for any  $t > 0$  and  $N > 0$ , by the definition of  $Z = X + Y$ , we have

$$\begin{aligned} \int_{-N}^N e^{t|z|} f_Z(z) dz &= \int_{-N}^N e^{t|z|} \int_{-\infty}^{\infty} f_X(z-y) f_Y(y) dy dz \\ &= \int_0^N e^{tz} \int_{-\infty}^{\infty} f_X(z-y) f_Y(y) dy dz + \int_0^N e^{tz} \int_{-\infty}^{\infty} f_X(-z-y) f_Y(y) dy dz \\ &\geq \int_{-\infty}^{\infty} e^{ty} f_Y(y) \int_0^N \left[ e^{t(z-y)} f_X(z-y) + e^{t(-z-y)} f_X(-z-y) \right] dz dy \\ &\geq \int_0^{\infty} e^{ty} f_Y(y) dy \int_{-N-y}^{N-y} e^{tx} f_X(x) dx, \end{aligned}$$

where we have used Fubini's theorem and change of variables. Letting  $N \rightarrow \infty$ , for any  $t > 0$  the final expression goes to infinity, which implies the claim and thus ends the proof.

**Acknowledgments.** CL would like to acknowledge helpful discussions with Yunan Yang. MD would like to thank Neil Chada and Alex Thiery for helpful discussions.

## REFERENCES

- [1] L. Ardizzone, J. Kruse, C. Rother and U. Köthe, Analyzing inverse problems with invertible neural networks, in *International Conference on Learning Representations*, 2019, URL <https://openreview.net/forum?id=rJed6j0cKX>.
- [2] M. Asim, M. Daniels, O. Leong, A. Ahmed and P. Hand, Invertible generative models for inverse problems: mitigating representation error and dataset bias, in *Proceedings of the 37th International Conference on Machine Learning* (eds. H. D. III and A. Singh), vol. 119 of *Proceedings of Machine Learning Research*, PMLR, 2020, 399–409.
- [3] A. Beskos, M. Girolami, S. Lan, P. E. Farrell and A. M. Stuart, Geometric MCMC for infinite-dimensional inverse problems, *Journal of Computational Physics*, **335** (2017), 327–351.
- [4] S. Borak, W. Härdle and R. Weron, *Stable Distributions*, 21–44, Springer Berlin Heidelberg, Berlin, Heidelberg, 2005.
- [5] T. Bui-Thanh, O. Ghattas, J. Martin and G. Stadler, A computational framework for infinite-dimensional Bayesian inverse problems part I: The linearized case, with application to global seismic inversion, *SIAM Journal on Scientific Computing*, **35** (2013), A2494–A2523.
- [6] H. Bölcskei, P. Grohs, G. Kutyniok and P. Petersen, Optimal approximation with sparsely connected deep neural networks, *SIAM Journal on Mathematics of Data Science*, **1**.
- [7] N. K. Chada, S. Lasanen and L. Roininen, Posterior convergence analysis of  $\alpha$ -stable sheets, 2019, ArXiv:1907.03086.
- [8] N. K. Chada, L. Roininen and J. Suuronen, Cauchy markov random field priors for Bayesian inversion, 2021, ArXiv:2105.12488.
- [9] A. Chambolle, M. Novaga, D. Cremers and T. Pock, An introduction to total variation for image analysis, in *Theoretical Foundations and Numerical Methods for Sparse Recovery*, 2010.
- [10] V. Chen, M. M. Dunlop, O. Papaspiliopoulos and A. M. Stuart, Dimension-robust MCMC in Bayesian inverse problems, 2019, ArXiv:1803.03344.
- [11] S. L. Cotter, M. Dashti and A. M. Stuart, Approximation of Bayesian inverse problems for PDEs, *SIAM Journal on Numerical Analysis*, **48** (2010), 322–345.
- [12] S. L. Cotter, G. O. Roberts, A. M. Stuart and D. White, MCMC methods for functions: modifying old algorithms to make them faster, *Statistical Science*, **28** (2013), 424–446.
- [13] M. Dashti, S. Harris and A. Stuart, Besov priors for Bayesian inverse problems, *Inverse Problems & Imaging*, **6** (2012), 183–200.
- [14] A. G. de G. Matthews, J. Hron, M. Rowland, R. E. Turner and Z. Ghahramani, Gaussian process behaviour in wide deep neural networks, in *International Conference on Learning Representations*, 2018, URL <https://openreview.net/forum?id=H1-nGgWC->.
- [15] R. Der and D. Lee, Beyond Gaussian processes: On the distributions of infinite networks, in *Advances in Neural Information Processing Systems* (eds. Y. Weiss, B. Schölkopf and J. C. Platt), MIT Press, 2006, 275–282, URL <http://papers.nips.cc/paper/2869-beyond-gaussian-processes-on-the-distributions-of-infinite-networks.pdf>.
- [16] J. N. Franklin, Well-posed stochastic extensions of ill-posed linear problems, *Journal of Mathematical Analysis and Applications*, **31** (1970), 682–716.
- [17] B. V. Gnedenko and A. N. Kolmogorov, *Limit distributions for sums of independent random variables*, Addison-Wesley Mathematics Series, Addison-Wesley, Cambridge, MA, 1954.
- [18] G. González, V. Kolehmainen and A. Seppänen, Isotropic and anisotropic total variation regularization in electrical impedance tomography, *Computers & Mathematics with Applications*, **74** (2017), 564–576.
- [19] M. Hairer, A. M. Stuart and S. J. Vollmer, Spectral gaps for a Metropolis–Hastings algorithm in infinite dimensions, *The Annals of Applied Probability*, **24** (2014), 2455–2490.
- [20] A. Immer, M. Korzepa and M. Bauer, Improving predictions of Bayesian neural nets via local linearization, in *AISTATS*, 2021, 703–711, URL <http://proceedings.mlr.press/v130/immer21a.html>.
- [21] J. Kaipio and E. Somersalo, *Statistical and Computational Inverse Problems*, Springer, Dordrecht, 2005, URL <https://cds.cern.ch/record/1338003>.
- [22] J. Kaipio and E. Somersalo, Statistical inverse problems: Discretization, model reduction and inverse crimes, *Journal of Computational and Applied Mathematics*, **198** (2007), 493–504.
- [23] B. Lakshminarayanan, A. Pritzel and C. Blundell, Simple and scalable predictive uncertainty estimation using deep ensembles, in *Proceedings of the 31st International Conference on Neural Information Processing Systems*, NIPS’17, 2017, 6405–6416.

- [24] M. Lassas, E. Saksman and S. Siltanen, Discretization-invariant Bayesian inversion and Besov space priors, *Inverse Problems & Imaging*, **3** (2009), 87–122.
- [25] M. Lassas and S. Siltanen, Can one use total variation prior for edge-preserving Bayesian inversion?, *Inverse Problems*, **20** (2004), 1537–1563.
- [26] M. Markkanen, L. Roininen, J. M. J. Huttunen and S. Lasanen, Cauchy difference priors for edge-preserving Bayesian inversion, *Journal of Inverse and Ill-posed Problems*, **27** (2019), 225–240.
- [27] R. M. Neal, *Priors for Infinite Networks*, 29–53, Springer New York, New York, NY, 1996.
- [28] J. Nocedal and S. J. Wright, *Numerical Optimization*, 2nd edition, Springer Verlag, Berlin, Heidelberg, New York, 2006.
- [29] R. Rahaman and A. H. Thiery, Uncertainty quantification and deep ensembles, 2020, ArXiv:2007.08792.
- [30] C. E. Rasmussen and C. K. I. Williams, *Gaussian Processes for Machine Learning (Adaptive Computation and Machine Learning)*, The MIT Press, 2005.
- [31] V. K. Rohatgi, *An Introduction to Probability and Statistics*, Wiley, New York, 1976.
- [32] C. Schillings, B. Sprungk and P. Wacker, On the convergence of the Laplace approximation and noise-level-robustness of Laplace-based Monte Carlo methods for Bayesian inverse problems, *Numerische Mathematik*, **145** (2020), 915–971.
- [33] A. M. Stuart, Inverse problems: A Bayesian perspective, *Acta Numerica*, **19** (2010), 451–559.
- [34] T. J. Sullivan, Well-posed Bayesian inverse problems and heavy-tailed stable quasi-Banach space priors, *Inverse Problems & Imaging*, **11** (2017), 857–874.
- [35] C. K. I. Williams, Computing with infinite networks, in *Proceedings of the 9th International Conference on Neural Information Processing Systems*, NIPS’96, MIT Press, Cambridge, MA, USA, 1996, 295–301.
- [36] Z.-H. Zhou, J. Wu and W. Tang, Ensembling neural networks: Many could be better than all, *Artificial Intelligence*, **137** (2002), 239–263.

E-mail address: [lichen@cims.nyu.edu](mailto:lichen@cims.nyu.edu)

E-mail address: [matt.dunlop@nyu.edu](mailto:matt.dunlop@nyu.edu)

E-mail address: [stadler@cims.nyu.edu](mailto:stadler@cims.nyu.edu)